

To appear in ApJ Letters

Iron Emission in $z \approx 6$ QSOs¹

Wolfram Freudling

*Space Telescope – European Coordinating Facility
European Southern Observatory
Karl-Schwarzschild-Str. 2
85748 Garching
Germany*

wfreudli@eso.org

Michael R. Corbin

*Science Programs, Computer Sciences Corporation
Space Telescope Science Institute
3700 San Martin Dr.
Baltimore, MD 21218*

corbin@stsci.edu

and

Kirk T. Korista

*Western Michigan University
Physics Department
1120 Everett Tower
Kalamazoo, MI 49008-5252*

kirk.korista@wmich.edu

ABSTRACT

We have obtained low-resolution near infrared spectra of three QSOs at $5.7 < z < 6.3$ using the NICMOS instrument of the Hubble Space Telescope. The spectra cover the rest-frame ultraviolet emission of the objects between $\lambda_{\text{rest}} \approx 1600 \text{ \AA} - 2800 \text{ \AA}$. The Fe II emission-line complex at 2500 \AA is clearly detected in two of the objects, and possibly detected in the third. The strength

of this complex and the ratio of its integrated flux to that of Mg II λ 2800 are comparable to values measured for QSOs at lower redshifts, and are consistent with Fe/Mg abundance ratios near or above the solar value. There thus appears to be no evolution of QSO metallicity to $z \approx 6$. Our results suggest that massive, chemically enriched galaxies formed within 1 Gyr of the Big Bang. If this chemical enrichment was produced by Type Ia supernovae, then the progenitor stars formed at $z \approx 20 \pm 10$, in agreement with recent estimates based on the cosmic microwave background. These results also support models of an evolutionary link between star formation, the growth of supermassive black holes and nuclear activity.

Subject headings: cosmology: observations — quasars: emission lines — quasars: individual (SDSS J083643.85 + 005453.3, SDSS J103027.10 + 052455.0, SDSS J104433.04 - 012502.2)

1. Introduction

The metallicities of high-redshift QSOs measured from their broad emission lines are an important probe of the young universe. These metallicities can be used to infer the properties of the QSO host galaxies, and to set limits on the formation of the first stars and supernovae (see the review by Hamann & Ferland 1999; Iwamuro et al. 2002, Dietrich et al. 2003). The recent discovery of QSOs at $z \approx 6$ (Fan et al. 2001; Fan et al. 2003) is of particular interest, as under currently favored cosmologies the age of the universe at such redshifts is approximately 1 Gyr, or only $\approx 7\%$ of its current value. Such an age approaches the formation timescale of the Type Ia supernovae that are the most likely source of QSO iron enrichment (see Hamann & Ferland 1999). Therefore, QSOs at $z \approx 6$ may begin to show significantly lower iron abundances than those at lower redshifts.

With these motivations, we have begun to obtain near-infrared spectra of QSOs at $z \approx 6$ discovered from the Sloan Digital Sky Survey (see Fan et al. 2001, 2003 and references therein) using the Near Infrared Camera and Multi-Object Spectrometer (NICMOS) of the Hubble Space Telescope. These NICMOS spectra cover a wider wavelength range than is possible from the ground because of telluric absorption. We are particularly interested

¹Based on observations made with the NASA/ESA Hubble Space Telescope, obtained at the Space Telescope Science Institute, which is operated by the Association of Universities for Research in Astronomy, Inc., under NASA contract NAS 5-26555. These observations are associated with proposal #9413.

in the measurement of the strength of the Fe II emission complex centered at a laboratory wavelength of 2500 Å, and the ratio of this emission to that of Mg II λ 2800, as this provides a diagnostic of the abundance ratio of iron to α -process elements, which in turn is an indicator of the occurrence of SNe Ia (see Hamann & Ferland 1999; Thompson et al. 1999; Iwamuro et al. 2002).

In this *Letter* we report the first results from this program. A detailed discussion of our data reduction procedures and a full modeling of the data are deferred to a later paper. Throughout this paper, we assume a cosmology of $H_o=71 \text{ km s}^{-1} \text{ Mpc}^{-1}$, $\Omega_\Lambda=0.73$, and $\Omega_m = 0.27$ (Bennett et al. 2003).

2. Observations and Data Reduction

Spectra of the three QSOs SDSS J083643.85+005453.3 ($z = 5.82$), SDSS J103027.10+052455.0 ($z = 6.28$), and SDSS J104433.04-012502.2 ($z = 5.78$) were obtained between 2002 October 25-27 using the G141 grism of the NICMOS instrument on the Hubble Space Telescope under GO program 9413. Hereafter, we refer to these sources as SDSS J1044-0125, SDSS J1030+0524 and SDSS J0836+0054. This grism covers the wavelength range from 1.1μ to 1.9μ with a nominal resolution of 200 per pixel. The final spectra represent the average of four individual spectra centered in each of the four NICMOS Camera 3 detector quadrants. Their position on the detector was changed in order to minimize the effect of large-scale and intra-pixel sensitivity variations in the detector on the co-added spectra. The total integration time for each spectrum was 2304 seconds. The spectra were extracted using the NICMOSlook software of Freudling (1997). Intra-pixel variations show up as a wavy pattern in individual spectra with an amplitude of approximately 8% of the mean flux level. The effect was corrected for during the extraction. The wavelength calibration of the spectra was derived from the observations of the planetary nebular HB12, and the flux calibration is based on the solar analog star P330-E (Freudling 2003) using a spectrum kindly provided by Rieke (2001). Galactic extinction at the position of the QSOs is negligible and was not corrected for.

3. Results

Our final spectra are shown in Figure 1, plotted as a function of observed and rest-frame wavelengths. The positions of the C III] λ 1909 and Mg II λ 2800 lines are marked with arrows, and the wavelength range of the main Fe II UV emission bump is marked with a

broad bar. The noise in the spectra is slightly correlated due to rebinning and flat-fielding uncertainties. The signal-to-noise ratios of our spectra are about 60 for SDSS J08364+0054 and SDSS J1044-0125, and about 30 for SDSS J1030+0524.

Each spectrum in Figure 1 is overplotted with the QSO composite spectrum of Zheng et al. (1997) derived from HST Faint Object Camera observations of objects in the approximate range $0.33 < z < 1.5$, shifted to the appropriate redshift. One can immediately see a basic correspondence between the continuum shapes of all three object spectra and that of the composite spectrum. In SDSS J0836+0054 and SDSS J1044-0125 one can also see the presence of the main UV Fe II emission bump and its correspondence to this feature in the composite. The detection of the Fe II emission bump in SDSS J1044-0125 is consistent with the detection of Fe II emission at $\lambda_{\text{rest}} \approx 3000 \text{ \AA}$ reported in this object by Aoki, Murayama & Denda (2002).

The spectrum of SDSS J1030+0524 is more ambiguous. The signal-to-noise ratio of this spectrum is the lowest of the three objects, adding to this uncertainty. There is an apparent absorption feature at approximately 1.57μ , which we also see in the four individual spectra, indicating that it is not a detector artifact. There are no objects nearby the QSO whose spectra could have contaminated it. We thus believe the feature to be real. It could represent a deep complex of Mg II $\lambda 2800$ narrow line absorbers at $z \approx 4.6$, or else be intrinsic to the QSO. The latter possibility might explain the apparent lack of strong emission in the Fe II complex, i.e., SDSS J1030+0524 might be related to the rare sub-class of QSOs showing Fe II absorption in their spectra (see Gregg et al. 2002 and references therein). A spectrum with a higher signal-to-noise ratio is required to resolve this uncertainty.

4. Measurement of the Fe II Emission Complex and Comparison with lower redshift QSOs

We measure the strength of the detected Fe II emission and its ratio to that in Mg II $\lambda 2800$ as follows. Following an approach first used by Wills, Netzer & Wills (1985; hereafter WNW85), we use a smoothed version of the composite spectrum of Zheng et al. (1997) as a template of the Fe II emission complex in the region $2250 \text{ \AA} - 2700 \text{ \AA}$ and extend it to both longer and shorter wavelengths using the theoretical Fe II template from WNW85 as a guide. We then model our NICMOS spectra as the combination of a continuum, our UV Fe II template, and Gaussian profiles. The continuum in our model consists of a power law with slope $\alpha = -0.33$ and a model Balmer continuum. All components are fitted simultaneously. The Mg II $\lambda 2800$ line in the QSO spectra is fitted by a single Gaussian profile, and the $\lambda 1900$ line blend that includes C III] $\lambda 1909$, Si III] $\lambda 1892$, and Al III $\lambda 1860$ is fitted as

two Gaussian profiles. In the case of SDSS J1030+0524, a third broader Gaussian profile is added to this blend to accommodate its shape. The redshift of the QSO is a free parameter in the fits, the resulting values are given in table 1. Fits to each spectrum are shown in Figure 2. While it can be seen from the plots that Mg II λ 2800 is incompletely covered in the spectra of SDSS J08364+0054 and SDSS J1044-0125, the shape of the line profiles suggest that the peak of the lines are within or very close to the wavelength range covered by our spectra. Fits to the blue sides of the profiles therefore allow a reasonable estimate of their total flux. For SDSS J1030+0524 where Mg II λ 2800 is not covered, we use the CIII] line blend instead and assume that $F(\text{Mg II}) = 1.37 \cdot F(\text{CIII])}$. The factor 1.37 is the mean flux ratio in radio-quiet QSOs (Brotherton et al. 1994).

The main source of uncertainty in the measured $F(\text{Fe II})$ is the value of the continuum slope. We therefore repeat our fitting procedure with different slopes between $\alpha = -0.30$ and -0.36 . For each slope, we judge by eye whether the fitted continuum corresponds to the measured flux values within their error bars and discard those which do not. Two of the remaining fits are shown for each object in Figure 2. We compute integrated fluxes $F(\text{Fe II})$ and $F(\text{Mg II})$ for each of the accepted continuum fits. We then take half the value of the difference between the maximum and minimum integrated flux as our error estimate. We note that for all continuum fits accepted during the inspection described above, we obtain a positive value for the integrated flux of the Fe II UV emission complex in SDSS J1030+0524. Nevertheless, because of the aforementioned ambiguity in our spectrum of this object, this value should only be considered an upper limit.

A more accurate measurement of the Fe II / Mg II ratio is possible in principle through the use of a Fe II template derived from the narrow-line QSO I Zw 1 (see Boroson & Green 1992; Corbin & Boroson 1996; Vestergaard & Wilkes 2001), but given our low spectral resolution, wavelength coverage and relatively low signal-to-noise ratios it is not clear that our data warrant this approach. However, we will test that method on our complete sample of spectra.

The integrated flux of the Fe II λ 2500 complex is generally measured over the wavelength range from 2150 to 3300 Å (e.g. WNW85), and the continuum fit is performed over the wavelength range from 1500 to 5000 Å. Our spectra however do not extend out this far in the object rest-frame, and therefore we can only measure the Fe II emission at wavelengths shorter than the Mg II line. In order to compare our measurements of the $F(\text{Fe II})/F(\text{Mg II})$ ratios to measurements of the same quantity in QSOs at lower redshifts by Iwamuro et al. (2002), we computed a scaled version of our Fe II/Mg II ratios,

$$[F(\text{Fe II})/F(\text{Mg II})]_{\text{scaled}} = s \times [F(\text{Fe II})/F(\text{Mg II})]_{\text{measured}}. \quad (1)$$

The scaling factor s was derived using our procedure to measure line fluxes on the template spectrum by Francis et al. (1991), for which Iwamuro et al. (2002) have reported a value for Fe II/Mg II of 4.26. We measure in this spectrum the Fe II/Mg II flux ratio using the same wavelength range, continuum regions, line and template fitting as for our NICMOS spectra. The final factor scaling s is chosen so that our scaled Fe II/Mg II flux ratio for the Francis spectrum is identical to the value quoted by Iwamuro et al. The measured and scaled values of this ratio are given in Table 1. While our measurement of the scaled Fe/Mg ratio in SDSS J1030+0524 is highly uncertain, a value near or above where we measure it would be consistent with the results of Pentericci et al. (2002), who from an analysis of the lines present in the optical spectrum of this object conclude that its metallicity is likely to be above the solar value.

Our measurement procedure is similar to those used by WNW85, Iwamuro et al. (2002) and Dietrich et al. (2002). Our scaling should therefore allow our measurements to be compared with theirs. In Figure 3 we plot our values in combination with the values listed by Iwamuro et al. (2002, their tables 2 and 3) and Dietrich et al. (2002, column “Fe II UV” of their table 4) as a function of redshift. The shaded region in this plot indicates the flux ratio of 2.75 ± 1.35 expected for solar abundances (see WNW85). The figure shows that the measured $F(\text{Fe II})/F(\text{Mg II})$ values are generally at or above this range of values, and more importantly show no trend with redshift over the range $z \approx 3 - 6.3$. All the QSOs in this combined sample have comparable luminosities. Thus while Iwamuro et al. (2002) find evidence for some redshift dependence of the Fe/Mg abundance ratio between high and low-redshift ($z \approx 0.1$) QSOs, the interpretation of this trend is complicated by the weak dependence of the Mg II $\lambda 2800$ equivalent width on continuum luminosity, and the wide luminosity range of their sample. There is thus no compelling evidence of evolution in QSO Fe/Mg abundance ratios from $z \approx 6$ to $z \approx 0.1$.

5. Discussion

The evidence that the objects in our sample have Fe/Mg abundance ratios at or above the solar value has several important implications. First, it supports models which predict that galaxy spheroids can reach solar or super-solar metallicities within ≈ 1 Gyr of their formation (e.g. Matteuchi 1994; Gnedin & Ostriker 1997; Romano et al. 2002). Second, the relationship between mass and metallicity found among local galaxies suggests that the hosts of these objects are very massive ($\sim 10^{11} - 10^{12} M_{\odot}$), possibly large elliptical galaxies (see Hamann & Ferland 1999). The presence of such galaxies at $z \approx 6$ would then support scenarios of an early formation epoch of massive galaxies (e.g. Cowie et al. 1996; Daddi,

Cimatti & Renzini 2000, Romano et al. 2002), as opposed to those in which they form via mergers at lower redshifts (e.g. Zepf 1997; Barger et al. 1999).

If the high metallicities suggested in our sample objects were produced by SNe Ia, then our assumed cosmology implies that these supernovae occurred less than 1 Gyr after the Big Bang. Their stellar progenitors must have evolved and gas must have sufficiently mixed before high Fe II/Mg II flux ratios are detectable. Matteucci & Recchi (2001) have shown that the formation timescale of SNe Ia is strongly dependent on environment, initial mass function, and star formation rate. Only several 100 Myr after the maximum SNe Ia rate does the gas Fe/Mg abundance ratio reach its solar values (Matteucci 1994). Recent models indicate that the time scale from the formation of SN Ia progenitor stars until the gas has been enriched ranges from 0.5 to 0.8 Gyr (Friaca & Terlevich 1998). The evidence of enrichment from SNe Ia at $z \approx 6$ thus indicates that the progenitor stars formed at $z \approx 20 \pm 10$. It is interesting to note that this range is similar to the range of re-ionization redshifts derived from the polarization fluctuations in the cosmic microwave background (Bennett et al. 2003). This would support the suggestion that stars rather than QSOs were mainly responsible for reionization (Yan, Windhorst & Cohen 2002).

It is likely that QSOs at $z \approx 6$ have only recently turned on. This is indicated mainly by their extremely low space density (see Shaver et al. 1996; Fan et al. 2003). Haiman & Cen (2002) conclude from the size of the ionized volume that SDSS J1030+052 has created in the surrounding neutral intergalactic medium, that it has been emitting at its observed luminosity for only $\sim 2 \times 10^7$ years. The evidence that star formation and supernovae began much earlier than the nuclear activity in these objects thus argues in favor of models proposing an evolutionary link between nuclear starbursts and the AGN phenomenon (Norman & Scoville 1988; Kauffmann & Haehnelt 2000; Kawakatu & Umemura 2003), as opposed to models in which the formation of supermassive black holes precedes that of galaxies. In the latter scenario, one would expect a more constant space density of QSOs at high redshifts along with an evolution in QSO metallicity (see Loeb 1993a; 1993b).

Acknowledgments. We dedicate this paper to the memory of the final crew of the Space Shuttle *Columbia*. The achievements of the Hubble Space Telescope would not be possible without the efforts of the dedicated astronauts of NASA, and we thank them for their service over the last thirteen years. We acknowledge useful discussion with Peter Shaver, and helpful comments by the referee Keith Thompson.

Support for proposal 9413 was provided by NASA through a grant from the Space Telescope Science Institute, which is operated by the Association of Universities for Research in Astronomy, Inc., under NASA contract NAS5-26555.

REFERENCES

- Aoki, K., Murayama, T., & Denda, K. 2002, PASJ, 54, 353
- Barger, A.J., Cowie, L.L., Trentham, N., Fulton, E., Hu, E.M., Songaila, A., & Hall, D. 1999, AJ, 117
- Bennett, C.L. et al. 2003, astro-ph/0302207
- Boroson, T.A. & Green, R.F. 1992, ApJS, 80, 109
- Brotherton, M.S., Tran, H.D., Becker, R.H., Gregg, M.D., Laurent-Muehleisen, S.A., & White, R.L. 2001, ApJ, 546, 775
- Brotherton, M.S., Wills, B.J., Steidel, C.C., & Sargent, W.L.W. 1994, ApJ 423, 131
- Corbin, M.R. & Boroson, T.A. 1996, ApJS, 107, 69
- Cowie, L.L., Songaila, A., Hu, E., & Cohen, J.G. 1996, ApJ, 112, 839
- Daddi, E., Cimatti, A., & Renzini, A. 2000, A&A, 362, 45
- Dietrich, M., Appenzeller, I., Hamann, F., Heidt, J., Jäger, K., Vestergaard, M., & Wagner, S.J. 2003, A&A, 398, 891
- Dietrich, M., Appenzeller, I., Vestergaard, M., & Wagner, S.J. 2002, ApJ, 564, 581
- Fan, X., et al., 2001, AJ, 122, 2833
- Fan, X. et al. 2003, astro-ph/0301135
- Francis, P.J., Hewett, P.C., Foltz, C.B., Chaffee, F.H., Weymann, R.J., & Morris, S.L. 1991, ApJ, 373, 465
- Freudling, W. 1997, ST-ECF Newsletter 24, 7
- . 2003, ST-ECF Newsletter 32, 16
- Friaca, A.C.S., & Terlevich, R.,J. 1998, MNRAS, 298, 399
- Gnedin, N.Y. & Ostriker, J.P. 1997, ApJ, 486, 581
- Gregg, M.D., Becker, R.H., White, R.L., Richards, G.T., Chaffee, F.H., & Fan, X. 2002, ApJ, 573, L85
- Haiman, Z., & Cen, R. 2002, ApJ, 578, 702

- Hamann, F., & Ferland, G. 1999, *ARA&A*, 37, 487
- Iwamuro, F., Motohara, K., Maihara, T., Kimura, M., Yoshii, Y., & Doi, M. 2002, *ApJ*, 565, 63
- Kauffmann, G. & Haehnelt, M. 2000, *MNRAS*, 311, 576
- Kawakatu, N. & Umemura, M. 2003, *ApJ*, 583, 85
- Loeb, A. 1993a, *ApJ*, 403, 542
- . 1993b, *ApJ*, 404, L37
- Matteucci, F. 1994, *A&A*, 288, 57
- Matteucci, F., & Recchi, S. 2001, *ApJ*, 558, 351
- Norman, C., & Scoville, N. 1988, *ApJ*, 332, 124
- Pentericci, L., et al 2002, *ApJ*, 123, 2151
- Rieke, M. 2001, private communication
- Romano, D., Silva, L., Matteuchi, F. & Danese, L. 2002, *MNRAS*, 334, 444
- Shaver, P.A., Wall, J.V., Kellermann, K.I., Jackson, C.A., & Hawkins, M.R.S. 1996, *Nature*, 384, 439
- Thompson, K.L., Hill, G.J., & Eston, R. 1999, *ApJ*, 515, 487
- Vestergaard, M. & Wilkes, B.J. 2001, *ApJS*, 134, 1
- Wills, B., Netzer, H., & Wills, D. 1985, *ApJ*, 288, 94 (WNW85)
- Yan, H., Windhorst, R. & Cohen, S.H. 2003, *ApJ*, 585, L93
- Yoshii, Y., Tsujimoto, T., & Kawara, K. 1998, *ApJ*, 507, L113
- Zepf, S.E. 1997, *Nature*, 390, 377
- Zheng, W., Kriss, G. A., Telfer, R. C., Grimes, J. P., & Davidsen A. F. 1997, *ApJ*, 475, 469

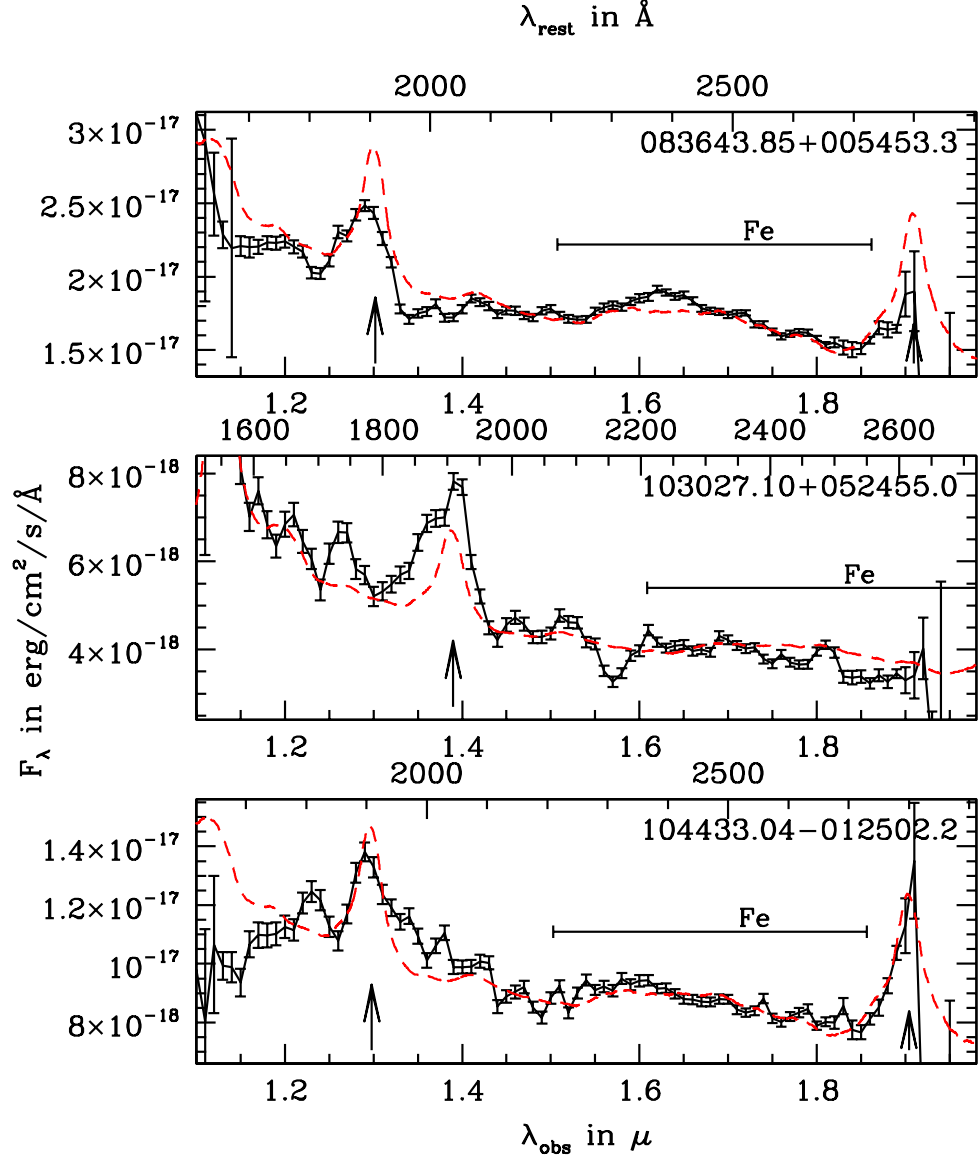


Fig. 1.— NICMOS spectra of our sample QSOs. The connected points are the NICMOS data. The error bars are the instrumental random errors. The wavelength range $2210 < \lambda_{\text{rest}} < 2730 \text{\AA}$ is labeled “Fe”. The expected positions of the C III] $\lambda 1909$, and Mg II $\lambda 2800$ lines are marked with arrows. The dashed lines show the scaled and redshifted composite spectrum of Zheng et al. (1997).

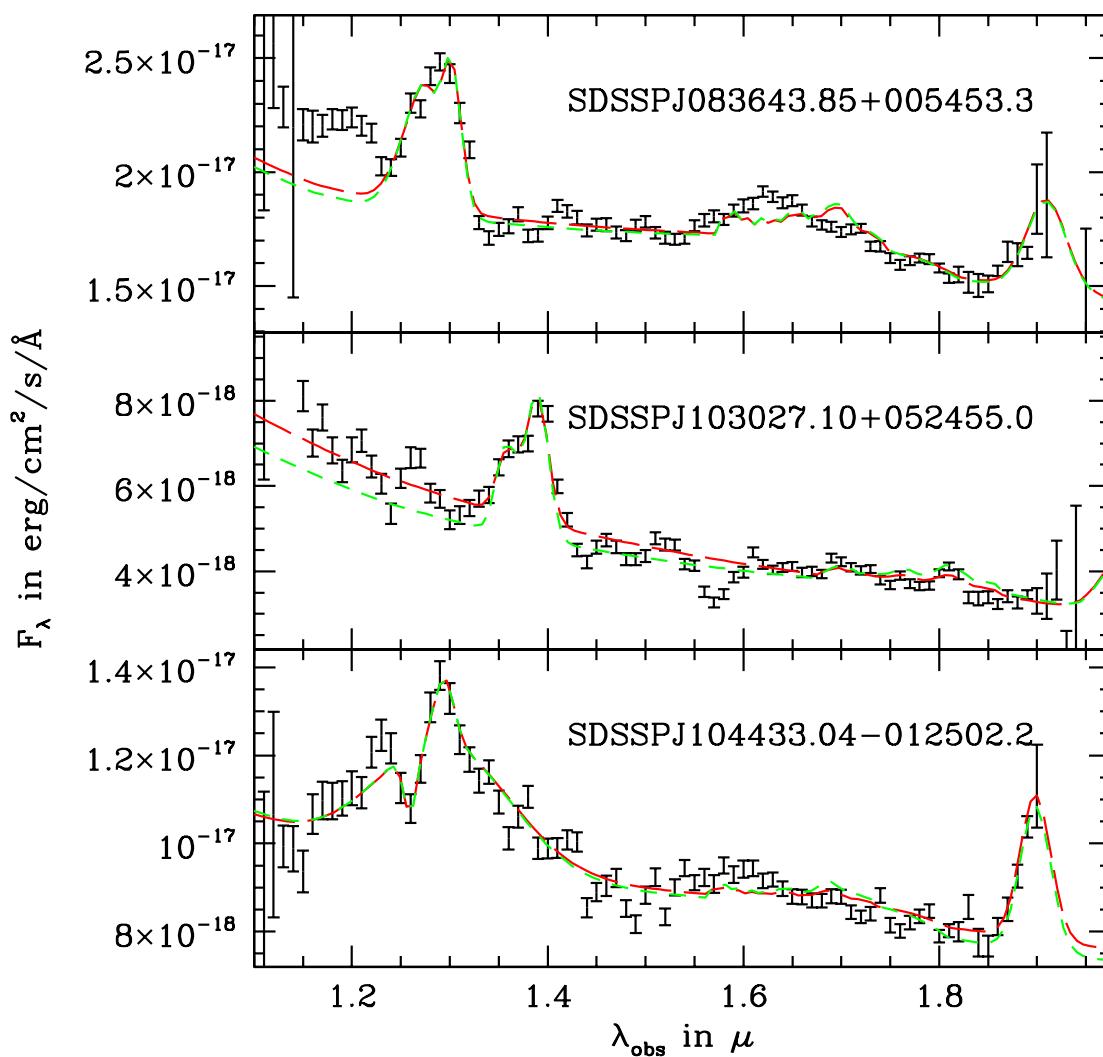


Fig. 2.— Fits of continuum, Fe II emission, and Mg II $\lambda 2800$ and C III] $\lambda 1909$ lines to our object spectra. The long-dashed and short-dashed lines show fits with different continuum slopes.

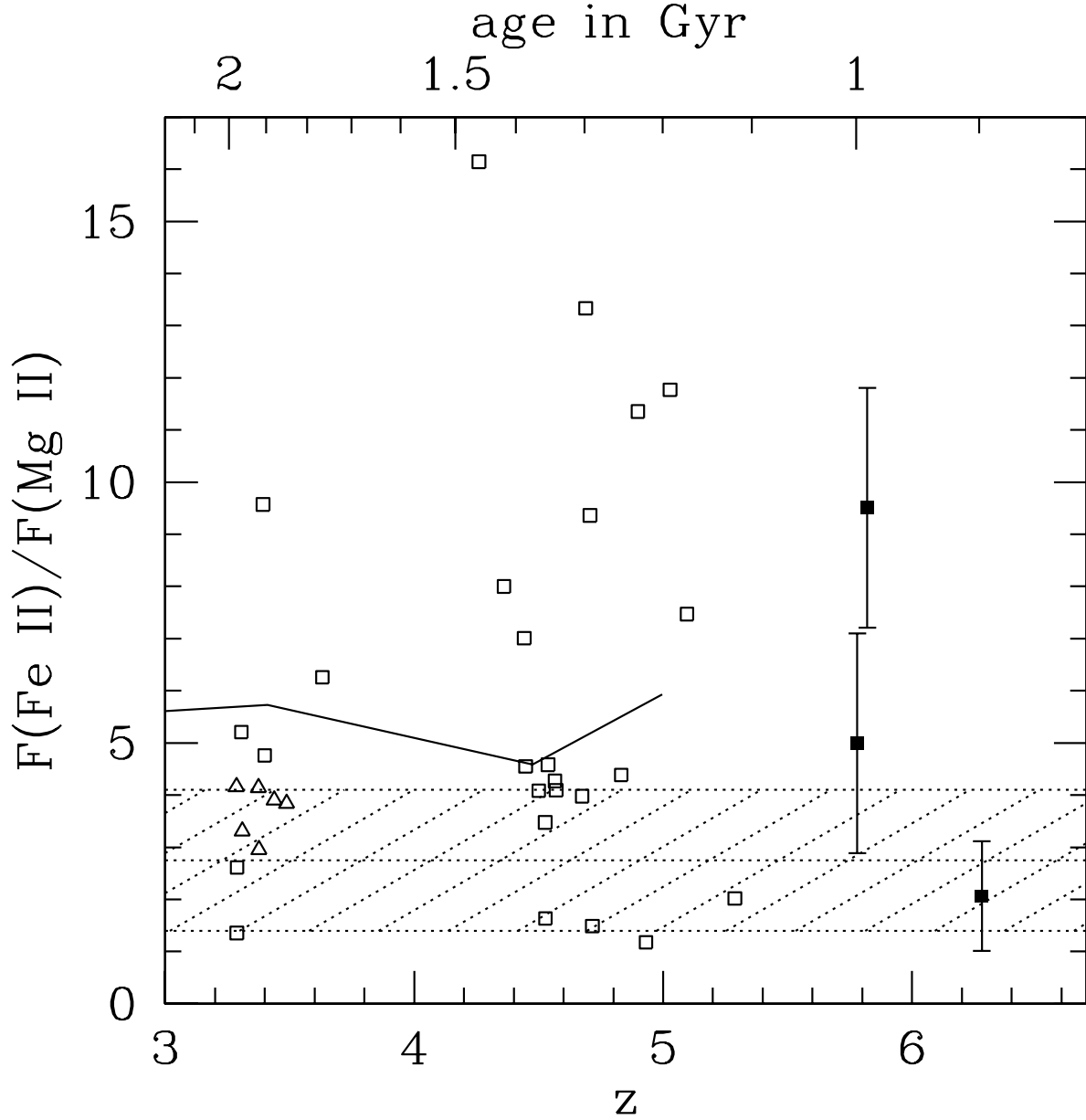


Fig. 3.— Integrated Fe II/Mg II flux ratios plotted as a function of redshift (lower axis) and age of the universe (upper axis). Open squares are data from Iwamuro et al. (2002), open triangles from Dietrich et al (2002), and solid squares from this work. The solid line shows the averages in redshift bins given by Iwamuro et al. (2002). The shaded area is the range of this ratio found by WNW85 to correspond to solar metallicity.

Table 1. Flux Ratios (Rest-Frame)

Source	z^a	F(Fe II)/F(Mg II) measured	F(Fe II)/F(Mg II) scaled
SDSS J0836+0054	5.82	5.41 ± 0.5	9.5 ± 2.3
SDSS J1030+0524	6.28	1.18 ± 0.5^b	2.1 ± 1.1
SDSS J1044-0125	5.78	2.84 ± 1.0	5.0 ± 2.1

^aRedshift as determined from fit of emission lines

^bF(Mg II) estimated from CIII] line blend